International Journal of Technology 13(1) 168-178 (2022)
Received September 2020 / Revised November 2020 / Accepted August 2021

International Journal of Technology

http://ijtech.eng.ui.ac.id

Preparation of a $NaFePO_4$ Cathode Material via Electrochemical Sodiation of $FePO_4$ Layers on Al Substrates

Fitria Rahmawati[1*], Dwi Aman Nur Romadhona[1], Desi Dyah Paramita[1], Witri Wahyu Lestari[2]

[1]*Research Group of Solid-State Chemistry & Catalysis, Chemistry Department, Universitas Sebelas Maret, Jl. Ir. Sutami 36 A Kentingan, Surakarta, 57126, Indonesia*
[2]*Research Group of Inorganic Materials, Chemistry Department, Universitas Sebelas Maret, Jl. Ir. Sutami 36 A Kentingan, Surakarta, 57126, Indonesia*

Abstract. In this research, a cyclic voltammetry (CV) method was applied to intercalate Na^+ into an $FePO_4$/Al substrate to produce $NaFePO_4$/Al as a potential cathode material. The sodiation was conducted directly to $FePO_4$ instead of applying delithiation to $LiFePO_4$ followed by sodiation, as was done in previous research. CV was conducted within a potential window of 2.0–4.0 V using a scan rate of 0.05 mVs^{-1}. The result was compared to $LiFePO_4$/Al treated with a similar method. The various scan rate was then applied to understand its effect on the electrochemical activity recorded in the voltammogram and its impedance profile. The results show that the CV product of $FePO_4$/Al (NFP(A)) was crystallized in an orthorhombic olivine $NaFePO_4$, as a result of Le Bail refinement. Orthorhombic $Na_{0.7}FePO_4$, trigonal FePO4, and monoclinic FePO4 were presented as secondary phases. Meanwhile, the CV product of $LiFePO_4$/Al (NFP(B)) was also crystallized in olivine $NaFePO_4$ and possessed secondary phases similar to NFP(A) with an additional Fe_2O_3 phase. NFP(A) showed two significant peaks at 2.442 V and 3.534 V, confirming sodiation/de-sodiation and Fe^{3+}/Fe^{2+} activity, respectively. Meanwhile, NFP(B) showed two peaks at 3.183 V and 3.04 V, corresponding to de-lithiation and sodiation, respectively. The Nyquist plots of both materials show a similar profile, with the impedance value of NFP(A) being lower than that of NFP(B). This confirms that the CV treatment of $FePO_4$/Al is more facile than the treatment of the $LiFePO_4$ layer, while also producing a cathode with higher electrical conductivity. Scan rate reduction to 0.04 mVs^{-1} produced a much lower impedance value, confirming higher electrical conductivity.

Keywords: Electrochemical Na insertion; Electrical properties; Sodium ion-battery; Sodium iron phosphate

1. Introduction

As important components in Lithium Ion-Batteries (LIBs), positive electrodes or cathodes have been studied for a few decades, with $LiFePO_4$ (LFP) attracting the most attention due to its favorable kinetics in the lithium intercalation/de-intercalation process (Li et al., 2015; Sofyan et al., 2016; Yang et al., 2013), the ease of controlling its size and shape (Boesenberg et al., 2013), its low cost, its high thermal safety, its good reversible capacity, its long cycle ability, and the fact that it is environmentally friendly (Popović, 2011). However, sustainable lithium supply is now a concern because lithium is usually

*Corresponding author's email: fitria@mipa.uns.ac.id, Tel.: +62-271-669376, Fax: +62-271-669376
doi: 10.14716/ijtech.v13i1.4306

only mined from limited deposits of Li_2CO_3 and LiOH (Kim et al., 2019). Sodium-Ion Batteries (SIBs) might be a good alternative for LIBs due to their high natural abundance and uniform geographic distribution on earth (Li et al., 2015; Wang et al., 2016).

Iron-based phosphates have been investigated as SIB cathodes, such as in the molecular forms of $Na_2FeP_2O_7$ (Kim et al., 2013), Na_2FePO_4F (Ellis et al., 2007), $Na_4Fe_3(PO_4)_2(P_2O_7)$ (Kim et al., 2012), $NaFePO_4$ (Kim et al., 2015), non-crystalline iron phosphate, $FePO_4$ (Liu et al., 2012), composites of amorphous $FePO_4$ nanospheres and carbon (Fang et al., 2014), and composites of $FePO_4$ nanospheres and graphene (Fan et al., 2014). Even though amorphous $FePO_4$ is easy to synthesize, olivine $NaFePO_4$ is preferable, especially for recently studied aqueous SIBs that require electrode materials to have operating potentials within the electrochemical stability window of water, in which H_2 and O_2 evolution should not occur (Jeong et al., 2019). The potential window should be between -0.83 V and 1.23 V vs. SHE at 25°C and 1 atm (Castellan, 1983). Meanwhile, maricite $NaFePO_4$ is not active electrochemically within 0–4.5 V due to cavities that trap Na ions and are not connected by pathways (Prosini et al., 2014). Further treatment to transform the maricite form into amorphous $NaFePO_4$ provides electrochemical activity within 1.5–4.5 V (Xiong et al., 2019). However, the potential window is above the potential window of aqueous SIB, which is in the range of -0.5–0.85 V (vs. Ag/AgCl) in 1 M aqueous $NaClO_4$ solution (Jeong et al., 2019).

$NaFePO_4$ can be conventionally synthesized through solid-state reactions using $FeC_2O_4.2H_2O$, Na_2CO_3, and $NH_4H_2PO_4$ as precursors, followed by calcination at 600°C for 10 h under an argon gas atmosphere (Kim et al., 2015). The maricite structure dominates the product. However, within the maricite structure, the diffusion channels of sodium ion transport are blocked (Heubner et al., 2017). Meanwhile, direct chemical synthesis appears to be unsuccessful for olivine $NaFePO_4$ preparation. Some researchers have produced olivine structures through ion-exchange methods using an organic-based electrochemical insertion into delithiated-$FePO_4$ (Oh et al., 2012; Avdeev et al., 2013; Galceran et al., 2014). This method requires two steps: de-lithiation and sodium insertion into the delithiated-$FePO_4$ in a new cell with sodium metal as the anode (Tang et al., 2016). The cyclic voltammetry profile of $FePO_4$ with $LiClO_4$ shows a single oxidation peak at 3.7 V and a single reduction peak at 2.85 V indicating de-lithiation/lithiation process of $LiFePO_4$ (Hansen et al., 2016). Meanwhile, when the $NaClO_4$ electrolyte was used, the peaks were at 3.65 V and 3.4 V, indicating de-lithiation of $LiFePO_4$ and then Na^+ insertion into the de-lithiated $LiFePO_4$. The diffusion of Na^+ into $FePO_4$ is slower than that of Li^+ (Heubner et al., 2016). This means that lithiation competes the Na^+ diffusion easily.

Therefore, in this research, the Na^+ intercalation was conducted directly to the $FePO_4$ layer without passing through a de-lithiation step. The $FePO_4$ was cast on an Al substrate to produce $FePO_4$/Al which was then used as a working electrode. Cyclic voltammetry mode was applied within 2.0–4.0 V of potential windows with a scan rate of 0.05 mVs^{-1}. A similar treatment was also conducted to $LiFePO_4$/Al for comparison. In addition, the effect of varying the scan rate effect was checked to determine the electrical properties of the materials.

2. Materials and Methods

2.1. Materials

The $FePO_4 \cdot 2H_2O$ (Sigma Aldrich, Singapore) powder was calcined at 700°C under argon gas (PT Samator Gas, Indonesia) flow before use. The calcined $FePO_4$ powder was then mixed with acetylene black (PT KGC, Indonesia) and polyvinylidene fluoride (PT KGC, Indonesia), with mass ratios of 70%, 20%, and 10%, respectively. The mixture was

dispersed in N-methyl-2-pyrrolidone (NMP) (PT KGC Indonesia), and then stirred until homogeneous. The slurry was cast on Al foil and dried at 60°C for 2 h in a vacuum oven. A similar treatment was also applied to the $LiFePO_4$ powder (MTI Corp., China) to produce $LiFePO_4$/Al.

2.2. The Electrochemical Sodiation

Electrochemical sodiation was conducted in a three-neck flask containing 50 mL of 1 M $NaClO_4$ electrolyte in propylene carbonate (analytical grade, Merck, Indonesia). The $FePO_4$/Al was used as the working electrode with Na metal (for synthesis, Merck, Indonesia) as the counter electrode. The reference electrode was Na metal. The electrodes were connected to a Corrtest CS150 electrochemical workstation (Corrtest, China) with a cyclic voltammetry mode of 2.0–4.0 V potential windows. The electrochemical cell was washed by allowing argon to flow for 5 min before operation.

After cyclic voltammetry, the sodiated $FePO_4$ (NFP(A)) was detached from the Al substrate. The NFP(A) powder was then heated to 470°C for 1 h under argon gas flow to remove the remaining $NaClO_4$ without destroying the olivine $NaFePO_4$ (Avdeev et al., 2013; US EPA, 2020).

2.3. Material Characterization

The synthesized-$NaFePO_4$ was characterized using X-ray Diffraction (XRD) (X-Pert PANalytical) equipped with RIETICA software for Le Bail refinement to identify the existing phases present and to predict the crystal structure and its cell parameters. Meanwhile, Scanning Electron Microscope/ Energy Dispersive X-ray (SEM/EDX) (JEOL JSM6510) analysis was conducted to understand the powder surface morphology. Electrical conductivity was investigated through impedance measurement with an Inductance-Capacitance-Resistance (LCR) meter (EUCOL U2826) by applying 0.2 V across a frequency range of 20 Hz to 5 MHz.

2.4. Electrochemical Analysis

For impedance measurement, a half-cell of $NaFePO_4$/Al was developed by applying a drop of $NaClO_4$ solution to the $NaFePO_4$/Al, followed by attaching the Al foil to cover the surface. This step was conducted within a glove box under an argon atmosphere. The half-cell was then vacuum sealed with an electric hot-press sealer. Both sides of the half-cell were attached with silver wire glued with silver paste. The $NaFePO_4$/Al side was connected to the positive pole, and the Al side was connected to the negative pole. A Nyquist plot of the measured-impedance Z, and the imaginary impedance Z'', was fitted using the ZView software (included in the Corrtest Electrochemical Workstation) to get the resistance value R. ZView fitting was used to determine R_{total} (ohm), the resistance value when Z'' is set to zero. Meanwhile, θ is the angle (radian), and Cdl is the double layer capacitance (Farad). The calculated R_{total} was then used to calculate the electrical conductivity σ (Scm^{-1}) (Rahmawati et al., 2019).

3. Results and Discussion

The calcined $FePO_4 \cdot 2H_2O$ shows a significant change in the XRD pattern compared to the initial $FePO_4 \cdot 2H_2O$, as seen in Figure 1a. Peaks at 2θ values of 27.60° and 58.52° (Figure 1b) confirm the presence of $FePO_4$ as they comply with the standard trigonal $FePO_4$ diffraction peaks (ICSD#412736). Meanwhile, peaks at 2θ values of 17.00°, 28.79°, 41.51°, 48.44°, and 53.00° comply with the peaks seen in the standard monoclinic $FePO_4$ diffraction pattern (ICSD#281079). Heat treatment also changed the surface morphology to larger particles with cleaned surfaces (Figure 1 insertion). EDX analysis found Fe, P, and O mass

contents of 44.11%, 18.37%, and 37.53%, respectively. Le Bail refinement found a trigonal $FePO_4$ P3121 that was crystallized within a volume cell of 269.912 $Å^3$ with the following lattice parameters: a = 5.20(2) Å, b = 5.20(2) Å, c = 11.44(4) Å. A monoclinic structure P121/n1 with the following cell parameters was also found: a = 5.57(2) Å, b = 7.62(2) Å, and c = 8.25(3) Å.

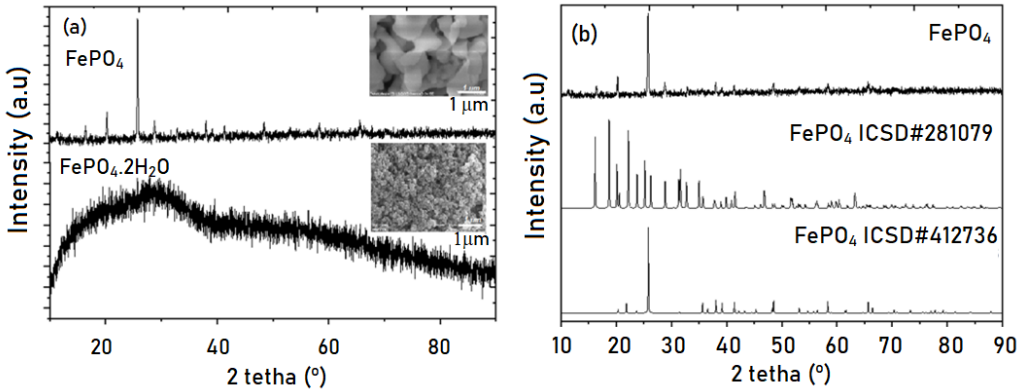

Figure 1 XRD patterns of: (a) $FePO_4 \cdot 2H_2O$ (bottom) and its calcined product $FePO_4$ (top); and (b) the XRD pattern of the experimental $FePO_4$ compared with standard $FePO_4$ XRD patterns (ICSD#412736 and ICSD #281079)

Electrochemical sodiation to the $FePO_4$ layer significantly changed the diffraction pattern, as presented in Figure 2, in which the peak intensity at $2\theta = 27.00^o$ decreased and some new peaks were revealed. Phase identification conducted using Le Bail refinement found that the new peaks fit well with orthorhombic $NaFePO_4$ and $Na_{0.7}FePO_4$, as described in the Le Bail plot in Figure 2c.

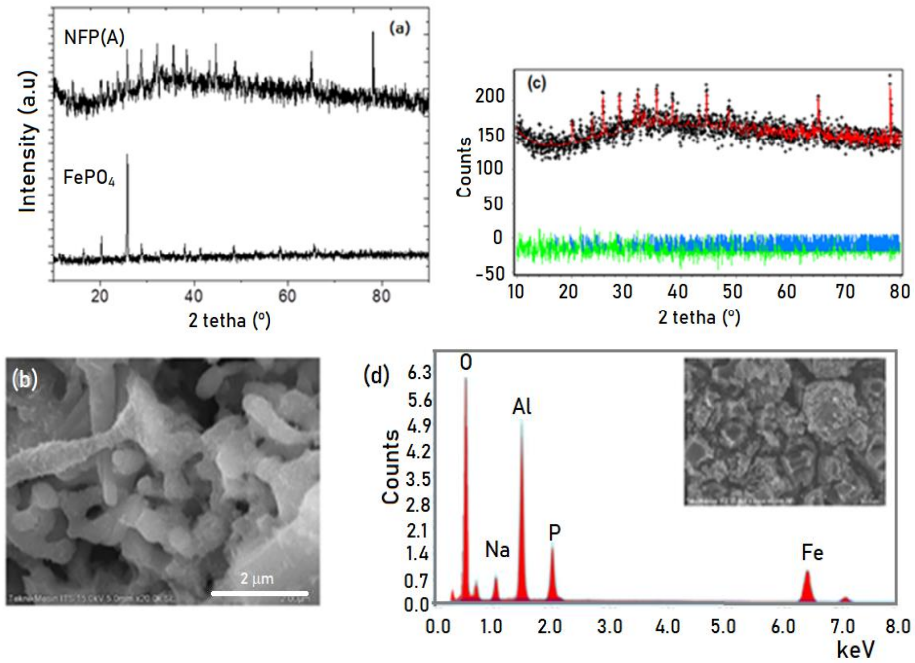

Elements	O (K)	Na (K)	Al (K)	P (K)	Fe (K)
Mass %	32.12	05.41	23.72	9.59	29.18
Error %	6.99	5.95	5.65	5.36	3.60
Atom %	50.77	9.88	22.23	7.83	13.21

Figure 2 (a) XRD patterns of $FePO_4$ and NFP(A)0.05 mVs^{-1}; (b) SEM images of NFP(A); (c) the Le Bail plot of NFP(A) by applying orthorhombic $NaFePO_4$ and orthorhombic $Na_{0.7}FePO_4$; and (d) the EDX result of NFP(A). The NFP(A)0.05 mVs^{-1} is the NFP produced via electrochemical sodiation of $FePO_4$ with 0.05 mVs^{-1} of scan rate

The diffraction pattern is similar to that seen in literature on NFP production, specifically the high peaks at 2θ values of 27°, 29°, and 22° (Oh et al., 2012). Some small peaks at 15°, 20°, 32°, 36°, 37°, 40°, and 48° are also found (Oh et al., 2012), instead of peaks at 57.0°, and 67.5° (Tang et al., 2017). Le Bail refinement confirms the presence of orthorhombic olivine $NaFePO_4$ (Moreau et al., 2010) and orthorhombic $Na_{0.7}FePO_4$. The presence of orthorhombic $Na_{0.7}FePO_4$ was also detected in previous research (Casas-Cabanas et al., 2012), and was recently confirmed as an ordered $Na_{2/3}FePO_4$ composition (Boucher et al., 2014). SEM analysis confirms that electrochemical sodiation changes the particle shape from spherical grains (Figure 1a) into connected grains, as described in Figure 2b. EDX analysis recorded the presence of 9.88% atoms with 5.95% of errors, which results in a calculated 9.88±0.294% atoms of Na (Ametek, 2020) (Figure 2d) inserted into $FePO_4$. The presence of Na inserted into $FePO_4$ was also proven by the XRD data, which showed that Na could be found in either orthorhombic $NaFePO_4$ or orthorhombic $Na_{0.7}FePO_4$. Al was also detected by EDX analysis (Figure 1d) as the $FePO_4$ film was cast on the Al substrate. The error percentage values were calculated by the TEAM-TM EDS software as a full calculation of analytical uncertainty and estimation of error propagation (Ametex, 2020).

The diffraction pattern of NFP(B) (Figure 3a) along with the Le Bail plot (Figure 3b) found that the diffraction pattern fit well with $Na_{0.7}FePO_4$ and $NaFePO_4$, however monoclinic $FePO_4$ was also found, and the Fe_2O_3 phase also existed. In fact, the Fe_2O_3 phase was also found in previous research on the synthesis of $NaFePO_4$ through the Pechini method (Sun et al., 2012). Le Bail refinement of XRD data found that cell parameters increased from $LiFePO_4$ (a = 10.326(1) Å, b= 6.0082(7) Å, c= 4.6878(6) Å, and cell volume = 290.83(6) $Å^3$) to $NaFePO_4$ (a = 10.682 Å, b = 6.290 Å, c = 5.138Å, and cell volume = 345.31081 $Å^3$).

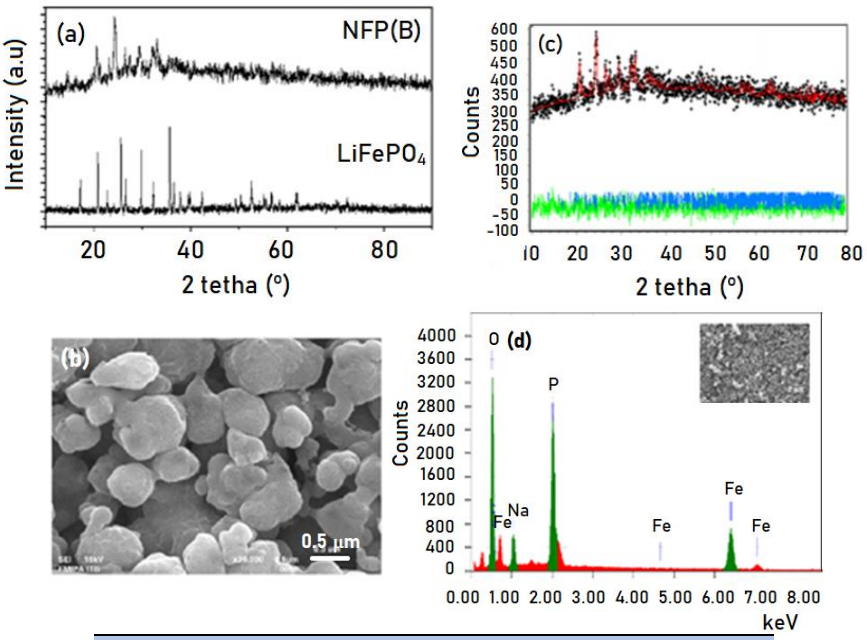

Elements	O(K)	Na(K)	P(K)	Fe(K)
Mass %	45.97	5.06	20.11	28.84
Error %	0.28	0.30	0.25	1.06
Atom %	67.45	5.18	15.24	12.12

Figure 3 (a) XRD patterns of $LiFePO_4$ and its electrochemical sodiation result NFP(B); (b) its SEM image; (c) the Le Bail plot by applying orthorhombic $NaFePO_4$ and orthorhombic $Na_{0.7}FePO_4$; and (d) its EDX results

The ~0.26–0.28 Å increase along the a and b axes corresponds to the replacement of Li (90 pm) with Na (110 pm). Meanwhile, Moreau et al. (2010) found a similar finding in their preparation of $NaFePO_4$ from $LiFePO_4$ with a potentiodynamic (PITT) mode, where a 0.2 Å increase was observed for the b and c axes (Moreau et al., 2010).

Cyclic voltammetry at 2.0–4.0 V did not completely transform the intermediate phase of $Na_{0.7}FePO_4$ into $NaFePO_4$. The intermediate $Na_{0.7}FePO_4$ was successfully isolated in previous research to study Na insertion/extraction to a commercial carbon-coated $LiFePO_4$, in which further sodiation was chemically carried out by NO_2BF_4 as an oxidizing agent and NaI as a reducing agent (Casas-Cabanas et al., 2012). Previous research confirmed that the $Na_{0.7}FePO_4$ is in the orthorhombic *Pnma* intermediate phase. The XRD patterns in this study matched those found in previous research. Casas-Cabanas et al. (2012) found that the cell parameters increase within the b [010] and a [100] directions after Na insertion, instead of along the c direction, as observed in electrochemically prepared samples (Moreau et al., 2010). Both findings indicate the probability of cell parameters increasing along the a, b, and c axes due to Na insertion, as it was also found within this study that the c cell parameter increases from 4.6878(6) Å in $LiFePO_4$ to 5.138 Å in NFP(B). Elemental analysis confirmed Na insertion by recording a 5.18% Na presence within the NFP(B) (Figure 3d).

Typical Nyquist plots of NFP (A) and NFP (B) are also similar (Figure 4b). ZView fitting determined the electrical conductivity of the materials to be 7.69×10^{-7} Scm^{-1} and 6.10×10^{-7} Scm^{-1} for NFP(A)0.05 and NFP(B)0.05, respectively (Table 1). Both instances are categorized as electrode-bulk interface conduction, based on their respective capacitance values of 7.69×10^{-7} F and 6.10×10^{-7} F, as a capacitance of 0.1 μF is considered the cut-off value for electrode-bulk interfaces (Martín et al., 2007; Apriyani et al., 2016; Rahmawati et al., 2021). The electrical conductivity is higher than today's leading cathode material, $LiFePO_4$, which has electrical conductivity as low as 10^{-9} Scm^{-1} (Amin et al., 2008), and 2×10^{-8} Scm^{-1} for $Li_3V_2(PO_4)_3$ (Yin et al., 2003) at room temperature.

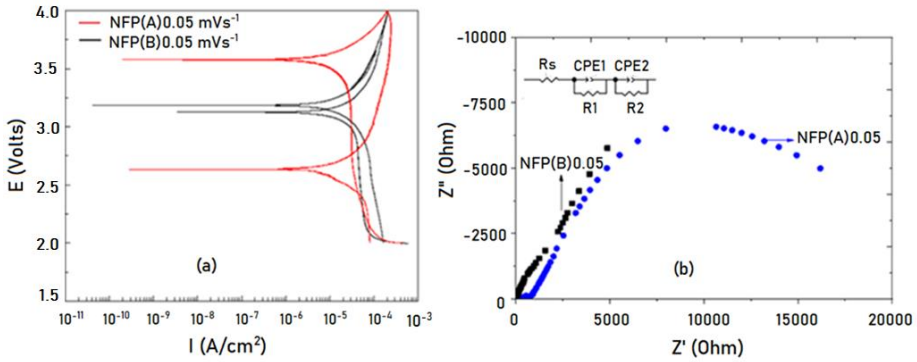

Figure 4 (a) CV curve of NFP(A)0.05 mV/s and NFP(B)0.05 mV/s; and (b) Nyquist plots of NFP(A) and NFP(B) along with their R-C network model

Table 1 Resistance and conductivity of Al | $NaFePO_4$ | $NaClO_4$ | Al for NFP(A) and NFP(B)

Material	R(Ω)	Capacitance (Farad)	Conductivity (Scm^{-1})	Chi square (χ^2) (Goodness of fit*)
NFP (A)0.04 mVs^{-1}	1242	1.95×10^{-7}	5.84×10^{-6}	0.399
NFP (A)0.05 mVs^{-1}	22251	7.69×10^{-7}	5.93×10^{-7}	0.019
NFP (A)0.2 mVs^{-1}	227960	1.22×10^{-7}	2.27×10^{-8}	0.665
NFP (B)0.05 mVs^{-1}	30590	2.69×10^{-6} 6.10×10^{-7}	1.75×10^{-7}	0.048
NFP(B)0.04 mVs^{-1}	4309	6.51×10^{-7}	1.79×10^{-6}	0.149

*Significant level is in between 0–1 (STAT TREK, 2020)

The volume expansion after Na insertion to $FePO_4$ to form $NaFePO_4$ is 12.999% (ΔV = 35.086Å^3), which is 2.69 times higher than the volume change of 4.836% for $Na_{0.7}FePO_4$ to $NaFePO_4$ formation (ΔV=14.748 Å^3). This is in agreement with previous research by Fang et al. (2015), who found that the volume expansion from $FePO_4$ to $Na_{2/3}FePO_4$ is three times larger than from $Na_{2/3}FePO_4$ to $NaFePO_4$ (Fang et al., 2015). It is known that by increasing the scan rate 10–40 times, the rate constant of $Na_{0.7}FePO_4$ formation increases, and two peaks are revealed within the oxidation and reduction parts. In this research, the increase in scan rate up to 0.2 mVs^{-1} also revealed two peaks at 2.48 V and 2.66 V (Figure 4), which is close to another result (Fang et al., 2017).

This research also applied a low scan rate of 0.04 mVs^{-1}, lower than the scan rate of 0.05 mVs^{-1} applied in other studies (Fang et al., 2015; Moreau et al., 2010), to understand the CV type when the current density was reduced to 4.259 x 10 $^{-8}$ Acm^{-2}. The peak split into two (Figure 5a), similar to NFP(A)0.05 mVs^{-1}; however, the second peak was revealed at a lower voltage of around 2.8 V. This probably indicates that one or both of Na^+/Na activation or Fe^{3+}/Fe^{2+} activation occurred and resulted in a higher electrical conductivity. Low current density seems to provide a low insertion/extraction rate which may produce a more regular structure with a low impedance value (Figure 5b). Further structural studies are required to deeply investigate this issue. In addition, low current density also revealed roughness peaks that probably came from multiple phases of the prepared $NaFePO_4$. Another study found that the presence of impurities in multi-walled carbon nanotubes plays an important role in catalyzing electrochemical reactions(Mustafa et al., 2018). Another study on metallic impurities within Double-Walls Carbon Nano Tubes (DWCNTs) also determined the effect of metals on the electrochemical response of the DWCNT electrode (Pumera and Iwai, 2009).

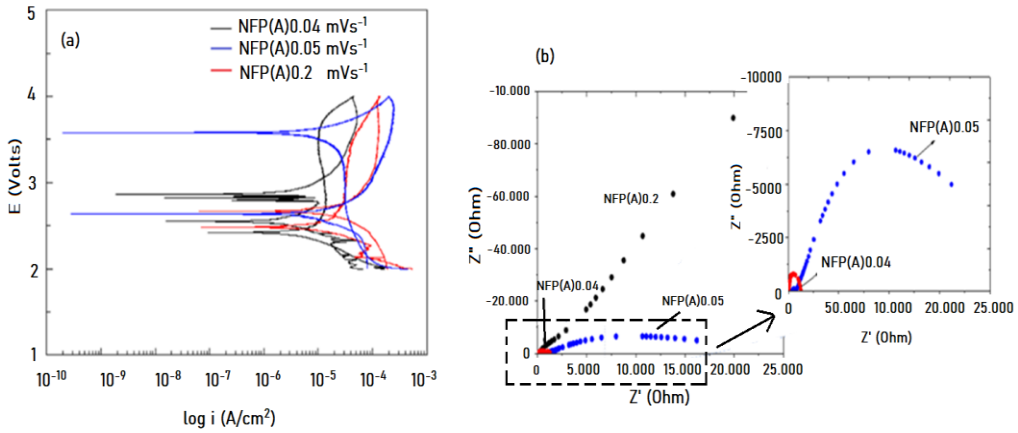

Figure 5 (a) Cyclic voltammogram of NFP(A) under different scan rates; and (b) their impedance plots

Nyquist plots in the range of 20 Hz–5 MHz (Figure 5b) show two semicircles without a spike line because spike lines are usually only revealed at very low frequencies below 20 Hz, as seen in the work of Zhu et al. (2013), which showed a spike line in a Nyquist plot of C-$NaFePO_4$ at recorded impedance frequencies as low as 10^{-3} Hz. The high-frequency semicircle is attributed to grains or particle-particle impedance or particle-to-current collector impedance (Illig et al., 2012; Zhu et al., 2013), while the middle frequency semicircle corresponds to charge transfer resistance (Illig et al., 2012). The semicircle of NFP(A)0.04 mVs^{-1} falls into a *Z'* value of 1242 Ω (Table 1), and the value is comparable to the impedance of mixed carbon $NaFePO_4$ (C-$NaFePO_4$) with the semicircle falling to a *Z''* value of around 1300 Ω (Zhu et al., 2013). This implies that NFP(A)0.04 mVs^{-1} is sufficient

for an electrochemical full cell. A similar rate of 0.04 mVs^{-1} was also applied to NFP(B) and produced a similar semicircle to that of NFP(A)0.04 mVs^{-1} with an impedance value of 4309 Ω, which was a significant reduction from 30590 Ω provided by NFP(B)0.05 mVs^{-1} (Table 1). It would be interesting for future work to optimize the electrochemical scan rate to find the highest conductivity of the NFP cathode.

4. Conclusions

Electrochemical sodiation was successfully applied in cyclic voltammetry mode to insert Na ions into the $FePO_4$ layer directly. This finding offers a simpler electrochemical method to insert/extract Na^+ directly as an alternative to the two-step de-lithiation and sodiation method. Impedance analysis even shows a similar semicircle trend, with a lower impedance value of $NaFePO_4$ from $FePO_4$, NFP(A), than the one prepared from the $LiFePO_4$ layer, NFP(B). This research also found that by reducing the scan rate to as low as 0.04 mVs^{-1}, the electrical conductivity increased for both NFP(A) and NFP (B).

Acknowledgements

This work was carried out with the financial support of the Hibah Penelitian Dasar 2019, The Ministry of Research, Technology, and Higher Education, the Republic of Indonesia, contract number 719/UN27.21/PN/2019.

References

Ametek, 2020. *TEAM TM EDS Software Suite*. AMETEX Materials Analysis Division. Available Online at https://www.edax.com/-/media/ametekedax/files/eds/product_bulletins/team eds software suite.pdf

Amin, R., Maier, J., Balaya, P., Chen, D.P., Lin, C.T., 2008. Ionic and Electronic Transport in Single Crystalline Lifepo4 Grown by Optical Floating Zone Technique. *Solid State Ionics*, Volume 179(27–32), pp. 1683–1687

Apriyani, K., Permadani, I., Syarif, D.G., Soepriyanto, S., Rahmawati, F., 2016. Electrical Conductivity of Zirconia and Yttrium-Doped Zirconia from Indonesian Local Zircon as Prospective Material for Fuel Cells. *In:* IOP Conference Series: Materials Science and Engineering; 10th Joint Conference on Chemistry, pp. 1–10

Avdeev, M., Mohamed, Z., Ling, C.D., Lu, J., Tamaru, M., Yamada, A., Barpanda, P., 2013. Magnetic Structures of $NaFePO_4$ Maricite and Triphylite Polymorphs for Sodium-Ion Batteries. *Inorganic Chemistry*, Volume 52(15), pp. 8685–8693

Boesenberg, U., Meirer, F., Liu, Y., Shukla, A.K., Dell'Anna, R., Tyliszczak, T., Chen, G., Andrews, J.C., Richardson, T.J., Kostecki, R., Cabana, J., 2013. Mesoscale Phase Distribution in Single Particles of $LiFePO_4$ Following Lithium Deintercalation. *Chemistry of Materials*, Volume 25(9), pp. 1664–1672

Boucher, F., Gaubicher, J., Cuisinier, M., Guyomard, D., Moreau, P., 2014. Elucidation of the $Na_2/_3FePO_4$ and $Li_2/_3FePO_4$ Intermediate Superstructure Revealing a Pseudouniform Ordering in 2D. *Journal of the American Chemical Society*, Volume 136(25), pp. 9144–9157

Casas-Cabanas, M., Roddatis, V.V., Saurel, D., Kubiak, P., Carretero-González, J., Palomares, V., Serras, P., Rojo, T., 2012. Crystal chemistry of Na Insertion/Deinsertion in $FePO_4$-$NaFePO_4$. *Journal of Materials Chemistry*, Volume 22(34), pp. 17421–17423

Castellan, G.W., 1983. *Physical Chemistry: Vol.* (R. . Rogers, M. Pinette, & J. Moore (eds.); Third Edition, Issue). Addison-Wesley Publishing Company, Inc

Ellis, B., Makahnouk, W., Makimura, Y., Toghill, K., Nazar, L., 2007. A Multifunctional 3.5 V

Iron-Based Phosphate Cathode for Rechargeable Batteries. *Nature Materials*, Volume 6(10), pp. 749–753

Fan, Q., Lei, L., Yin, G., Chen, Y., Sun, Y., 2014. Electrochemistry Communications Direct Growth of $FePO_4$/Graphene Hybrids for Li-Ion and Na-Ion Storage. *Electrochemistry Communications*, Volume 38, pp. 120–123

Fang, Y., Liu, Q., Xiao, L., Ai, X., Yang, H., Cao, Y., 2015. High-Performance Olivine $NaFePO_4$ Microsphere Cathode Synthesized by Aqueous Electrochemical Displacement Method for Sodium Ion Batteries. *ACS Applied Materials and Interfaces*, Volume 7(32), pp. 17977–17984

Fang, Y., Xiao, L., Qian, J., Ai, X., Yang, H., Cao, Y., 2014. Mesoporous Amorphous $FePO_4$ Nanospheres as High-Performance Cathode Material for Sodium-Ion Batteries. *Nano Letters*, Volume 14(6), pp. 3539–3543

Fang, Y., Zhang, J., Xiao, L., Ai, X., Cao, Y., Yang, H., 2017. Phosphate Framework Electrode Materials for Sodium Ion Batteries. *Advanced Science*, Volume 4(5), pp. 1–21

Galceran, M., Saurel, D., Acebedo, B., Roddatis, V.V., Martin, E., Rojo, T., Casas-Cabanas, M., 2014. The Mechanism of $NaFePO_4$ (de)Sodiation Determined by in Situ X-Ray Diffraction. *Physical Chemistry Chemical Physics*, Volume 16(19). https://doi.org/10.1039/c4cp01089b

Hansen, S., Quiroga-gonzález, E., Carstensen, J., Föll, H., 2016. Size-Dependent Cyclic Voltammetry Study of Silicon Microwire Anodes for Lithium Ion Batteries. *Electrochimica Acta*, Volume 217, pp. 283–291

Heubner, C., Heiden, S., Matthey, B., Schneider, M., Michaelis, A., 2016. Electrochimica Acta Sodiation vs. Lithiation of $FePO_4$: A Comparative Kinetic Study. *Electrochimica Acta*, Volume 216, pp. 412–419

Heubner, C., Heiden, S., Schneider, M., Michaelis, A., 2017. In-Situ Preparation and Electrochemical Characterization of Submicron Sized $NaFePO_4$ Cathode Material for Sodium-Ion Batteries. *Electrochimica Acta*, Volume 233, pp. 78–84

Illig, J., Ender, M., Chrobak, T., Schmidt, J.P., Klotz, D., Ivers-Tiffée, E., 2012. Separation of Charge Transfer and Contact Resistance in $LiFePO_4$-Cathodes by Impedance Modeling. *Journal of the Electrochemical Society*, Volume 159(7), pp. 952–960

Jeong, S., Hoon, B., Don, Y., Yeon, C., Mun, J., Tron, A., 2019. Artificially Coated $NaFePO_4$ for Aqueous Rechargeable Sodium-Ion Batteries. *Journal of Alloys and Compounds*, Volume 784, pp. 720–726

Kim, D.H., Kim, M.Y., Yang, S.H., Ryu, H.M., Jung, H.Y., Ban, H., Park, S., Lim, J.S., Kim, H., 2019. Fabrication and Electrochemical Characteristics of NCM-Based All-Solid Lithium Batteries using Nano-Grade Garnet Al-LLZO Powder. *Journal of Industrial and Engineering Chemistry*, Volume 71, pp. 445–451

Kim, H, Park, I., Seo, D., Lee, S., Kim, S., Kwon, W., Park, Y., Kim, C., Jeon, S., Kang, K., 2012. New Iron-Based Mixed-Polyanion Cathodes for Lithium and Sodium Rechargeable Batteries: Combined First Principles Calculations and Experimental Study. *Journal of American Chemical Society*, Volume 134(25), pp. 19369–10372

Kim, Heejin, Shakoor, R., Park, C., Lim, S.Y., Kim, J.S., Jo, Y.N., Cho, W., Miyasaka, K., Kahraman, R., Jung, Y., Choi, J.W., 2013. $Na_2FeP_2O_7$ as a Promising Iron-Based Pyrophosphate Cathode for Sodium Rechargeable Batteries: A Combined Experimental and Theoretical Study. *Advanced Functional Materials*, Volume 23(9), pp. 1147–1155

Kim, J., Seo, D.-H., Kim, H., Park, I., Yoo, J.-K., Jung, S.-K., Park, Y.-U., Goddard III, W.A., Kang, K., 2015. Unexpected Discovery of Low-Cost Maricite $NaFePO_4$ as a High-Performance Electrode for Na-Ion Batteries. *Energy & Environmental Science*, Volume 8(2), https://doi.org/10.1039/C4EE03215B

Li, C., Miao, X., Chu, W., Wu, P., Tong, D.G., 2015. Hollow Amorphous $NaFePO_4$ Nanospheres as a High-Capacity and High-Rate Cathode for Sodium-Ion Batteries. *Journal of Materials Chemistry A*, Volume 3(16), pp. 8265–8271

Liu, Y., Xu, Y., Han, X., Pellegrinelli, C., Zhu, Y., Zhu, H., Wan, J,. 2012. Porous Amorphous $FePO_4$ Nanoparticles Connected by Single-Wall Carbon Nanotubes for Sodium Ion Battery Cathodes. *Nano Letter,* Volume 12(11), pp. 5664–5668

Martín, P., López, M.L., Pico, C., Veiga, M.L., 2007. $Li_{(4-x)/3}Ti_{(5-2x)/3}Cr_xO_4$ ($0 \leq x \leq 0.9$) Spinels: New Negatives for Lithium Batteries. *Solid State Sciences*, Volume 9(6), pp. 521–526

Moreau, P., Guyomard, D., Gaubicher, J., Boucher, F., 2010. Structure and Stability of Sodium Intercalated Phases in Olivine $FePO_4$. *Chemistry of Materials*, Volume 22(14), pp. 4126–4128

Mustafa, I., Al, A., Al, A., Susantyoko, R., 2018. Effects of Carbonaceous Impurities on the Electrochemical Activity of Multiwalled Carbon Nanotube Electrodes for Vanadium Redox Flow Batteries Effects of Carbonaceous Impurities on the Electrochemical Activity Of Multiwalled Carbon Nanotube Electrodes For. *Carbon*, Volume 131, pp. 47–59

Oh, S.M., Myung, S.T., Hassoun, J., Scrosati, B., Sun, Y.K., 2012. Reversible $NaFePO_4$ Electrode for Sodium Secondary Batteries. *Electrochemistry Communications*, Volume 22(1), pp. 149–152

Popović, J., 2011. *Novel Lithium Iron Phosphate Materials for Lithium-ion Batteries.* Master's Thesis, Graduate Program, Universität Potsdam, Germany

Prosini, P.P., Cento, C., Masci, A., Carewska, M., 2014. Sodium Extraction from Sodium Iron Phosphate with a Maricite Structure. *Solid State Ionics*, Volume 263, pp. 1–8

Pumera, M., Iwai, H., 2009. Multicomponent Metallic Impurities and Their Influence Upon the Electrochemistry of Carbon Nanotubes. *Journal of Physical Chemistry C*, Volume 113(11), pp. 4401–4405

Rahmawati, F., Kusumaningtyas, A.A., Saraswati, T.E., Prasetyo, A., Suendo, V., 2021. Mn-doped $NaFeO_2$ from a Low Purity-Fe Precursor and its Performance as Cathode for Sodium-Ion Battery. *Inorganic and Nano-Metal Chemistry*, Volume 51(3), pp. 383–390

Rahmawati, F., Zuhrini, N., Nugrahaningtyas, K.D., Arifah, S.K., 2019. Yttria-stabilized zirconia (YSZ) Film Produced from an Aqueous Nano-YSZ Slurry: Preparation and Characterization. *Journal of Materials Research and Technology*, Volume 8(5), pp. 4425–4434

Sofyan, N., Putro, D., Zulfia, A., 2016. Performance of Vanadium-doped $LiFePO_4$/C used as a Cathode for a Lithium Ion Battery. *International Journal of Technology*, Volume 7(8), pp. 1307–1315

STAT TREK., 2020. *Chi-Square Goodness of Fit Test*. Statistic Dictionary. Available Online at https://stattrek.com/statistics/dictionary.aspx?definition=chi-square goodness of fit test

Sun, A., Beck, F.R., Haynes, D., Poston, J.A., Narayanan, S.R., Kumta, P.N., Manivannan, A., 2012. Synthesis, Characterization, and Electrochemical Studies of Chemically Synthesized $NaFePO_4$. *Materials Science and Engineering B: Solid-State Materials for Advanced Technology*, Volume 177(20), pp. 1729–1733

Tang, H., Wang, M., Lu, T., Pan, L,. 2017. Porous Carbon Spheres as Anode Materials for Sodium-Ion Batteries with High Capacity and Long Cycling Life. *Ceramics International*, Volume 43(5), pp. 4475–4482

Tang, W., Song, X., Du, Y., Peng, C., Lin, M., Xi, S., Tian, B., Zheng, J., Wu, Y., Pan, F., Loh, K.P. 2016. High-Performance $NaFePO_4$ Formed by Aqueous Ion-Exchange and its Mechanism for Advanced Sodium Ion Batteries. *Journal of Materials Chemistry A,*

Volume 4(13), https://doi.org/10.1039/C6TA01111J

US EPA., 2020. *Sodium Perchlorate 7601-89-0 | DTXSID1034185*. DSSTox Substance Id. Available Online at https://comptox.epa.gov/dashboard/dsstoxdb/results?search=DTXSID1034185#properties

Wang, S., Xia, L., Yu, L., Zhang, L., Wang, H., Low, X., 2016. Free-Standing Nitrogen-Doped Carbon Nanofiber Films: Integrated Electrodes for Sodium-Ion Batteries with Ultralong Cycle Life and Superior Rate Capability. *Advanced Energy Materials*, Volume 6(7), ttps://doi.org/10.1002/aenm.201502217

Xiong, F., An, Q., Xia, L., Zhao, Y., Mai, L., Tao, H., Yue, Y., 2019. Revealing the Atomistic Origin of the Disorder-Enhanced Na-Storage Performance in $NaFePO_4$ Battery Cathode. *Nano Energy*, Volume 57, pp. 608–615

Yang, J., Wang, J., Tang, Y., Wang, D., Li, X., Hu, Y., Li, R., Liang, G., Sham, T.K., Sun, X., 2013. $LiFePO_4$-Graphene as a Superior Cathode Material for Rechargeable Lithium Batteries: Impact of Stacked Graphene and Unfolded Graphene. *Energy and Environmental Science*, Volume 6(6), pp. 1521–1528

Yin, S.C., Grondey, H., Strobel, P., Anne, M., Nazar, L.F., 2003. Electrochemical Property: Structure Relationships in Monoclinic Li_3-y$V_2(PO_4)_3$. *Journal of the American Chemical Society*, Volume 125(34), pp. 10402–10411

Zhu, Y., Xu, Y., Liu, Y., Luo, C., Wang, C., 2013. Comparison of Electrochemical Performances of Olivine $NaFePO_4$ in Sodium-Ion Batteries and Olivine $LiFePO_4$ in Lithium-Ion Batteries. *Nanoscale*, Volume 5(2), pp. 780–787